mathematics

MDPI

Article

Modeling and Simulation for Non-Motorized Vehicle Flow on Road Based on Modified Social Force Model

Jiaying Qin, Sasa Ma *, Lei Zhang, Qianling Wang and Guoce Feng

School of Artificial Intelligence and Data Science, Hebei University of Technology, Tianjin 300401, China
* Correspondence: masasa2022@163.com

Abstract: Non-motorized vehicles have become one of the most commonly used means of transportation for people due to their advantages of low carbon, environmental protection, convenience and safety. Frequent interaction among non-motorized vehicle users in the shared space will bring security risks to their movement. Therefore, it is necessary to adopt appropriate means to evaluate the traffic efficiency and safety of non-motorized vehicle users in the passage, and using a micro model to conduct simulation evaluation is one of the effective methods. However, some existing micro simulation models oversimplify the behavior of non-motorized vehicle users, and cannot reproduce the dynamic interaction process between them. This paper proposes a modified social force model to simulate the dynamic interaction behaviors between non-motorized vehicle users on the road. Based on the social force model, a new behavioral force is introduced to reflect the three dynamic interaction behaviors of non motor vehicle users, namely, free movement, following and overtaking. Non-motorized vehicle users choose which behavior is determined by the introduced decision model. In this way, the rule-based behavior decision model is combined with the force based method to simulate the movement of non-motorized vehicles on the road. The modified model is calibrated using 1534 non-motorized vehicle trajectories collected from a road in Xi'an, Shaanxi, China. The validity of the model is verified by analyzing the speed distribution and decision-making process of non-motorized vehicles, and comparing the simulation results of different models. The effects of the number of bicycles and the speed of electric vehicles on the flow of non-motorized vehicles are simulated and analyzed by using the calibrated model. The relevant results can provide a basis for urban management and road design.

Keywords: non-motorized vehicles; social force model; dynamic interaction behavior; behavioral force model

MSC: 37M05

Citation: Qin, J.; Ma, S.; Zhang, L.; Wang, Q.; Feng, G. Modeling and Simulation for Non-Motorized Vehicle Flow on Road Based on Modified Social Force Model. *Mathematics* **2023**, *11*, 170. https://doi.org/10.3390/math11010170

Academic Editors: Costin Badica, Nick Bassiliades, Kalliopi Kravari and Theodoros Kosmanis

Received: 7 November 2022
Revised: 15 December 2022
Accepted: 21 December 2022
Published: 29 December 2022

1. Introduction

As a primary means of transportation, non-motorized vehicles have been widely promoted in many countries due to their public health and environmental benefits. The safety of non-motorized users and the construction of non-motorized infrastructure have also been widely promoted in these countries [1]. However, as the demand for non-motorized vehicles increases, it also brings many bottlenecks related to traffic management [2]. Since the riding space is shared in the non-motorized lane, the operating space between the non-motorized users is ambiguous, which leads to frequent interaction between the non-motorized users at different speeds, which poses serious problems for the safety and efficiency of road traffic [3]. Thus, accurate evaluation is needed to help design and manage passageways for non-motorized vehicles. Non-motorized vehicle micro-simulation models are a great way to meet this need [4].

Generally, the non-motorized vehicle flow micro-simulation models can be divided into two categories: cellular automata (CA) and social force models (SFM). The cellular

automaton model can simulate the spatiotemporal evolution of complex systems. Tang et al. [5] proposed an extended cellular automata model to study the movement of each pedestrian in the university canteen. Every pedestrian's movement within the university canteen is flawlessly replicated by considering the characteristics of the pedestrian flow within the university canteen and the characteristics of the university canteen. Liang et al. [6] used a cellular automata model to simulate pedestrian flow to avoid collisions during evacuation. At the same time, they used the proposed CA model considering collision avoidance to explore the impact of collision avoidance on the evacuation process. Cao et al. [7] proposed a cellular automaton simulation model for the space-time distribution of mixed bicycles. Based on the updated rules of the NaSch model, the conflict between heterogeneous bicycles and dynamic lane-changing behaviors in two-dimensional space was considered. At the same time, the proposed mesh density and time step of the model have been upgraded. The CA model cannot show cyclic dynamics in two-dimensional space because it is affected by discrete motion, which does not happen in real life [8].

The discipline of evacuation has conducted substantial research on social force models, which can account for movements in continuous space. Li et al. [9] proposed a speed correction method that considered the interaction between human attributes and different groups of people and discussed the influence of different human attributes and different personnel on evacuation efficiency in the case of a passenger ship fire. Deng et al. [10] proposed a dynamic route optimization method based on an improved real-time information algorithm to obtain the optimal evacuation route when a fire broke out on a cruise ship. Huang et al. [11] used the social group force model to model how people act within and between groups. Han et al. [12] introduced an information transfer mechanism into a social force model to simulate the behavior of pedestrians in emergencies. Guo et al. [13] improved the social force model by introducing the force generated by the green signal countdown and analyzed the characteristics of pedestrians crossing the road twice. Qin et al. [14] proposed a group vision-sharing method and added aggregation and collective collision avoidance force to the original social force formula to simulate two-way pedestrian flow. Even though the social force model has been extensively studied in human behavior, it has not gotten as much attention in the non-motorized sector.

Recently, Zhou et al. [15] proposed a new data fusion method to explore the impact of shared electric bicycles on space-time commuting demand by fusing multi-source data such as shared electric bicycle travel data, traffic communities and building environments. Li et al. [16] explored how members of bicycle groups interact and organize in bicycle flows, which has important implications for bicycle traffic modeling and safe bicycle facility design. Liu et al. [17] proposed a new force model for simulating evacuation in complex environments that considers more environmental factors, making it suitable for complex emergency environments. Liu et al. [18] propose an agent-space model (ASM) to elucidate the movement of cyclists and pedestrians on shared roads, accounting for the dispersion observed among non-motorized road users. Anvari et al. [19] proposed a three-level micro-mathematical model capable of representing the behavior of pedestrians and vehicles in a shared spatial layout and implemented it in a traffic simulation tool. Luo et al. [20] studied mixed pedestrian–bicycle merging flows at T-junctions under symmetric and asymmetric merging situations, which supports the design of mixed traffic facilities and the management of pedestrian-bicycle flows. Schöttl et al. [21] used an individual-based model to simulate the behavior of crowds to estimate evacuation times and crowd density and optimize the efficiency of public transport. Some studies [22–24] expand the force range by adding specific collision avoidance/behavior forces or changing parameters based on the simulation implementation, which is often beneficial to make the model more closely related to the dynamic behavior of traffic users. In practice, however, the behavioral processes are intricate and beyond the capabilities of force-based models [25]. Therefore, additional elements need to be introduced to the force-based model to ensure the fidelity of the simulation results. Anvari et al. [19] integrated additional path-planning models into the force-based model to provide traffic users with global pathfinding. Liang et al. [26] put

rule-based behavioral constraints into a force-based model to simulate how people interact in traffic.

This study designs a modified non-motorized vehicle SFM model that integrates the behavioral decision-making behavior of non-motorized vehicle users. The main contributions of this study are as follows:

- In the original SFM model, we introduced a behavioral force model, which involves three common interaction behaviors of non-motorized vehicles, namely, free movement, following and overtaking.
- The model was calibrated using trajectory data collected in Xi'an, Shanxi, China, and satisfactory performance was obtained. Simulations are used to determine how the number of bikes in the road affects the average speed of electric vehicles.

The structure of this paper is as follows. Section 2 introduces the modified social force model and the specific implementation method. Section 3 presents data acquisition and processing, model calibration and comparison of simulation results. Finally, Section 4 summarizes the findings and proposes future research directions.

2. Methods

In this section, we first discuss the general idea and structure of the proposed model in Section 2.1 and then illustrate the decision model of the proposed model in Section 2.2, which includes the decisions for free-moving, following and overtaking behaviors. Finally, the calculation of specific behavioral forces is discussed in Section 2.3.

2.1. Modified Social Force Model

We chose the original SFM [27] as the basis for the non-motorized vehicle microsimulation model because it considers the user's continuous motion.

In the original SFM, the dynamics of an object are captured by a driving force and repulsive forces exerted by other road users [22]. The driving force motivates the object to move freely toward the destination at its desired speed. The repulsive force represents the expectation of maintaining a safe distance from other road users. In addition, a special repulsive force is exerted by the boundaries of infrastructure, such as fences and markers, defined as boundary forces, which are usually introduced to limit the extent of the area an object can reach. The basic structure of the original SFM is shown in Figure 1a.

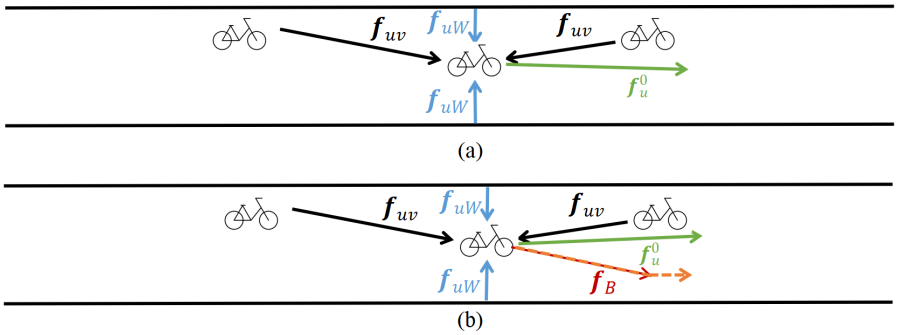

Figure 1. Comparison of the original SFM and the modified SFM. (**a**) The original SFM. (**b**) The modified SFM.

The resultant force of the original SFM is presented as follows:

$$m_u \frac{dv_u(t)}{dt} = f_u^0(t) + \sum_{v(\neq u)} f_{uv}(t) + \sum_W f_{uW}(t) - \xi_u(t) \quad (1)$$

The left side of Equation (1) represents the resultant instantaneous force on the object in the form of Newton's second law, where u represents the non-motorized vehicle individually; m_u represents the mass of the individual u; t represents the time variable;

and $v_u(t)$ represents, at the time of t, the actual speed of the individual u. The right side of the equal sign is the sum of the various forces received by the individual, where $f_u^0(t)$ represents the force generated by personal u to drive itself in the target direction; $f_{uv}(t)$ represents the repulsive force between individuals u and v; the direction of the force is from the individual v to individual u; $f_{uW}(t)$ represents the repulsion between individuals u and the boundary; and $\xi_u(t)$ represents the disturbance force produced by the individual u under the effect of numerous factors.

The original SFM lacks an additional decision mechanism to ensure sufficient realism of non-motorized vehicle interaction behavior [22]. In addition, non-motorized vehicles typically exhibit three behavioral choices in non-motorized traffic: free movement, following and overtaking [28]. For accurate simulation, the decision model that considers the above three behaviors should also be added to the original SFM.

We modified the original SFM by embedding an element to describe the interactive decision process, as shown in Figure 1b. We build a behavioral force model with a decision-making process in which decision outcomes are selected based on the decision model and implemented by the corresponding behavioral force. The decision model aims to choose the appropriate behavior among three options: free movement, following and overtaking. The decision model captures the dynamic behavior and interactions of non-motor vehicles, bringing the model simulation results closer to reality. Therefore, compared with Equation (1), the behavioral force f_B is introduced into the original SFM. The resultant force of the modified SFM can be expressed by Equation (2).

$$m_u \frac{dv_u(t)}{dt} = f_u^0(t) + \sum_{v(\neq u)} f_{uv}(t) + \sum_W f_{uW}(t) + f_B - \xi_u(t) \tag{2}$$

This revised model's repulsive, boundary and driving forces are consistent with the original SFM. Equations (3) and (4) can be used to describe the social force f_{uH} between the simulated object u and other interactive objects H (including other traffic users v and boundary W).

$$f_{uH} = A_{uH} \exp\left(\frac{-d_{uH}}{B_{uH}}\right) n_{uH} k_{uH} \tag{3}$$

$$k_{uH} = \left[\lambda + (1-\lambda)\frac{1+\cos(\varphi_{uH})}{2}\right] \tag{4}$$

In the equation, d_{uH} is the distance between the simulated object u and other interacting objects H, as shown in Figure 2; n_{uH} is the unit vector of H pointing to u; k_{uH} is the anisotropy of the interaction, which is related to the angular difference φ_{uH} between H the moving direction and u the moving direction; A_{uH} and B_{uH} are parameters to be estimated; and parameter λ represents φ_{uH} the degree of influence from 0 to 1. More details can be found in Helbing and Molnar's study [19].

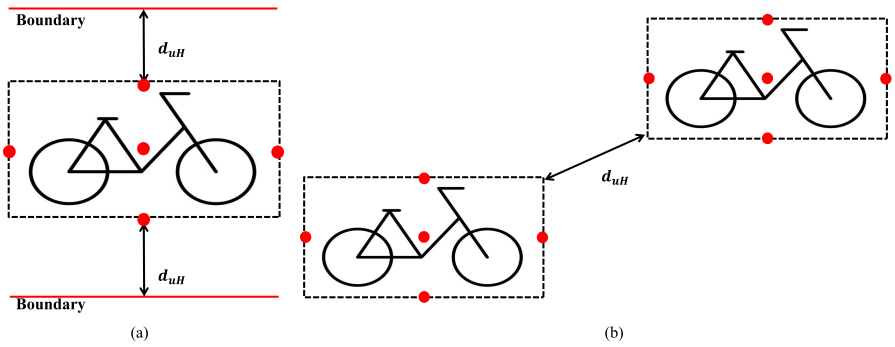

Figure 2. The concept of d_{uH}. (**a**) The distance between non-motorized vehicles and the boundary. (**b**) The distance between non-motorized vehicles and non-motorized vehicles.

2.2. Decision for Free Movement, Following and Overtaking Behaviors

This paper assigns a rule-based algorithm to make behavioral decisions at each time step. Rule-based time steps will give an appropriate behavioral decision outcome (i.e., free movement, following and overtaking). The factors considered in this algorithm are the non-motorized vehicle decision parameters commonly used in the literature [29], such as speed and position relationship. The definition of the positional relationship of interactive objects is shown in Figure 3.

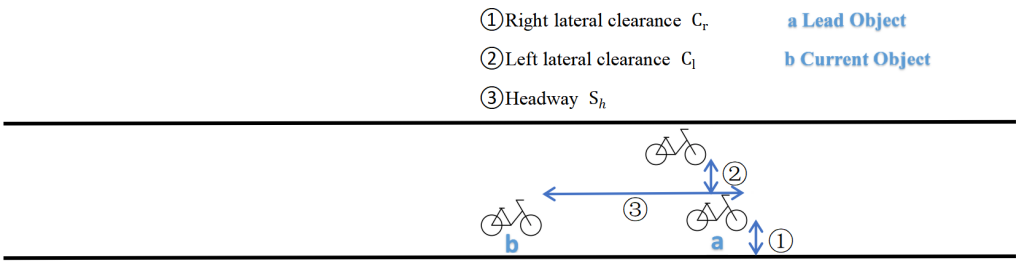

Figure 3. Schematic diagram of parameters related to following/overtaking decision/free movement decision.

Here, the way to figure out which object is in front and which is behind is described in the literature [30], and the method can be written as Equation (5):

$$\left|y_v(t) - y_g(t)\right| \leq \frac{1}{2} w_v \tag{5}$$

Among them, $y_v(t)$ denotes the lateral position of the current rider; $y_g(t)$ represents other objects' lateral position; g represents a leading or lagging object selected from all front and rear road users; and w_v equals the current rider's width and a different shy-away distance. Among them, the shy-away distance is defined as the additional lateral distance. Since the shy-away distance represents the free lateral space ahead of the cyclist who needs to ride [30], its value is set to 0.5 m, which is the half-width of the cyclist. (Jin's research [31] shows that the non-motorized vehicle width is set at 1.00 m).

The specific flow of the algorithm is shown in Figure 4. In addition to the given parameters shown in Figure 3, $v_v(t)$ represents the current speed of the non-motorized vehicle; $v_{v+1}(t)$ represents the current speed of the leading object. In addition, several numerical examples with different types of the leading object and corresponding decision results are provided in Table 1. These examples show that cyclists will choose appropriate behavior in their current traffic conditions.

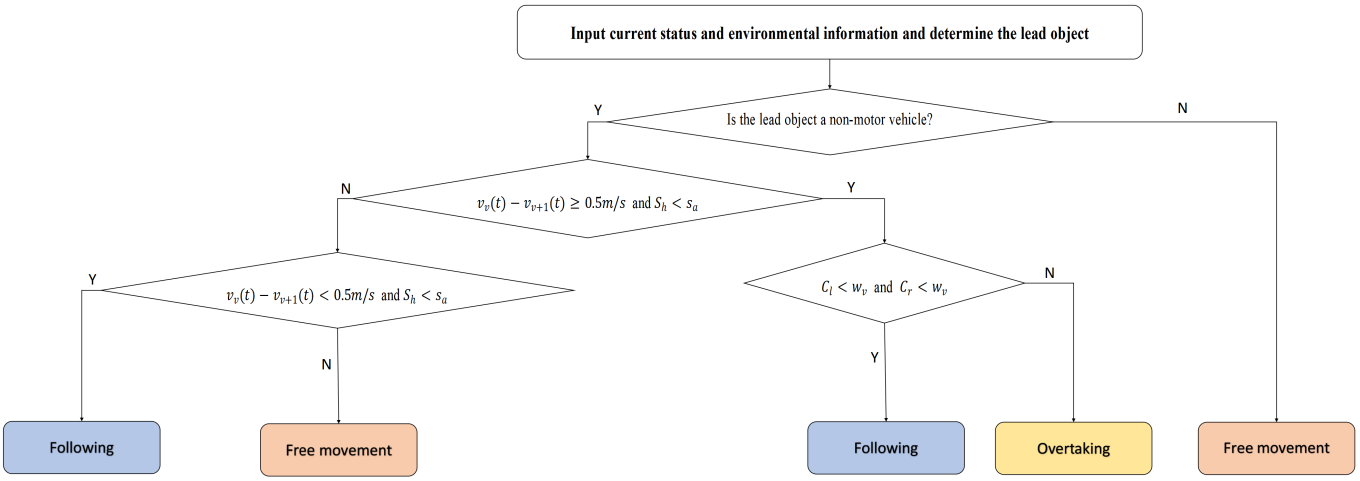

Figure 4. Determining free movement, following and overtaking behavior at one time step.

Table 1. Numerical examples of decision-making algorithms.

	$v_v(t)$(m/s)	$v_{v+1}(t)$(m/s)	$S_h(s)$	$C_l(m)$	$C_r(m)$	**Decision Result**
Have leading object	6.31	3.36	1.29	2.07	0.43	Overtaking
	5.54	4.43	1.96	0.32	0.58	Following
Others	-	-	-	-	-	Free movement

2.3. Behavior Force Model

A specific behavior corresponds to a behavioral force model to calculate the corresponding force. As mentioned above, there are three basic behaviors: free movement, following and overtaking.

If the behavioral decision model selects a specific behavior in a simulation time step, the corresponding force model is dedicated to calculating its behavioral force. Cyclists interact with other cyclists by determining intermediate destinations based on selected behaviors [32].

The direction of the behavioral force points to an intermediate destination corresponding to a particular behavior. Among them, the intermediate destination of the free movement behavior is set as the final destination of the cyclist, which is a random position outside the passage's exit. A follow-behavior object's intermediate destination is at its lead object's tail. The intermediate destination of the overtaking behavior is located at the side of the overtaken non-motorized vehicle, maintaining a fixed distance from the overtaken non-motorized vehicle. Among them, the fixed distance required for overtaking is determined by the actual data overtaking lateral displacement distance. Figure 5 displays the schematic representations of the intermediate locations for the three behavioral force models used in this study.

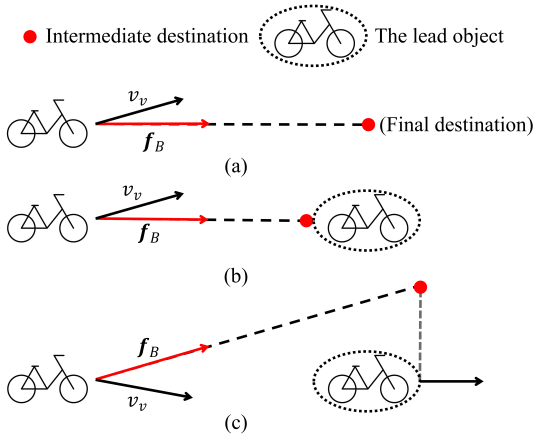

Figure 5. Intermediate destination for free movement, following and overtaking actions. (**a**) Free movement-driving force. (**b**) Following behavior-following force. (**c**) Overtaking behavior-overtaking force.

The specific models of free movement, following and overtaking behaviors are constructed as follows:

2.3.1. The Free Movement Force Model

This study uses the forward driving force of the original SFM as the operational model that powers the free-motion behavior. The free-moving behavior force f_B calculation is expressed by Equations (6) and (7):

$$f_B(t) = m_v \frac{v_d e_d - v_v}{\tau_d} \tag{6}$$

$$\boldsymbol{e}_d(t) = \frac{r_v^d - r_v}{\left| r_v^d - r_v \right|} \tag{7}$$

Among them, v_d represents the desired speed; τ_d is the relaxation time; v_V is the current speed; $\boldsymbol{e}_d(t)$ represents the desired direction; r_v^d is the intermediate destination; and r_v is the current simulated non-motorized vehicle instantaneous position. For the following behavioral force equation, the calculation of $\boldsymbol{e}_d(t)$ is consistent.

2.3.2. The Bicycle-Following Force Model

The following force model is represented by the Intelligent Driver Model (IDM) developed by Treiber et al. [33], which is believed to simulate non-motorized vehicle following behavior [34] effectively. The following behavior force $\boldsymbol{f}_B$ calculation is represented by Equations (8) and (9):

$$\boldsymbol{f}_B(t) = m_v a_{\max} \cdot \left(1 - \left(\frac{v_v}{v_d} \right)^{\delta_e} - \left(\frac{S_d}{\Delta S} \right)^2 \right) \cdot \boldsymbol{e}_d(t) \tag{8}$$

$$S_d = s_0 + s_1 \cdot \sqrt{\frac{v_v}{v_d}} + T_d \cdot v_v + \frac{v_v \cdot \Delta v}{2\sqrt{a_{\max} \cdot b_f}} \tag{9}$$

where $a_{\max}$ is the maximum acceleration of the simulated non-motorized vehicle; δ_e is the acceleration index; S_d is the desired minimum distance; and ΔS is the distance between two vehicles measured from the leading edge of the current non-motorized vehicle to the rear of the previous non-motorized vehicle; and s_0, s_1 is the distance of the jam; T_d is the time interval of the safety time; Δv is the speed difference with the previous non-motorized vehicle; and b_f is a comfortable deceleration.

2.3.3. The Overtaking Force Model

To simplify the complexity of the model, we decouple the overtaking behavior forces in the lateral and longitudinal directions and consider the component forces in these two directions separately. According to the work of Ni, the force of these two components is calculated as follows: the Equation (10), which calculates the force of the longitudinal component of $\boldsymbol{f}_B^x$, and Equation (11), which calculates the force of the transverse component of $\boldsymbol{f}_B^y$.

$$\boldsymbol{f}_B^x(t) = (-0.12 \cdot \Delta s + 0.72) \cdot \boldsymbol{e}_x(t) \tag{10}$$

$$\boldsymbol{f}_B^y(t) = \frac{y_d}{n} * \frac{\pi}{(t_0)^2} \cdot \cos\left(\frac{t_0 - t'}{t_0} \cdot \pi \right) \cdot \boldsymbol{e}_y(t) \tag{11}$$

Δs represents the longitudinal separation between the current non-motorized vehicle and the overtaken non-motorized vehicle; y_d represents the expected lateral offset of the current non-motorized vehicle in the corresponding stage; t_0 represents the duration of each stage; $\boldsymbol{e}_x(t)$ and $\boldsymbol{e}_y(t)$ represent the longitudinal and lateral directions; and n represents a parameter.

3. Case Study

3.1. Data

Because the simulation model proposed in this paper reproduces the traffic situation in the road through the cyclist's decision making on its behavior, testing on non-motorized lanes with frequent interactions is required. The research site is selected as a non-motorized vehicle lane named Weiyang Road in Xi'an, Shanxi, China. The non-motorized vehicle flow passing through this road comprises electric vehicles and bicycles. In this scene, the interaction between the cyclists is clear, and the direction of their movement changes a lot.

Currently, the target tracking algorithm based on Yolov5 and Deep Sort is the best method for extracting video trajectory data, which can realize functions such as traffic statistics, trajectory tracking and speed detection. Cameras were set up at nearby heights

to get a full view of the non-motorized vehicle. The video was collected from around 17:30 to 19:30 on 25 September 2022, and the weather conditions during the investigation were clear. We obtained 1534 non-motorized vehicle trajectories in videos with 0.03 s intervals, including 346 bicycles and 1188 electric vehicle trajectories, and the localization accuracy of the trajectories is 0.05 m.

3.2. Model Calibration

In addition to the measurable parameters v_d, y_d and t_0, the genetic algorithm (GA) was used to obtain the optimal values of the relevant parameters of the modified SFM force model. Let v_d be the average value y_d and t_0 of the vehicle speed distribution in the empirical data for bicycles and electric vehicles, respectively. According to bicycles overtaking bicycles, electric vehicles overtaking electric vehicles, bicycles overtaking electric vehicles, and electric vehicles overtaking bicycles, it is set as the average value of the vehicle overtaking lateral displacement and overtaking time in the empirical data. The objective function is set according to the free movement, following and overtaking behaviors of the vehicle, such as Equations (12)–(14):

$$RMSPE_1 = \sqrt{\frac{\sum_{t=1}^{M}\sum_{i=1}^{N}\left(Y_{it}^{sim} - Y_{it}^{obs}\right)^2}{\sum_{t=1}^{M}\sum_{i=1}^{N}\left(Y_{it}^{obs}\right)^2}} \tag{12}$$

$$RMSPE_2 = \sqrt{\frac{\sum_{t=1}^{M}\sum_{i=1}^{N}\left(X_{it}^{sim} - X_{it}^{obs}\right)^2}{\sum_{t=1}^{M}\sum_{i=1}^{N}\left(X_{it}^{obs}\right)^2}} \tag{13}$$

$$RMSPE_3 = \sqrt{\frac{\sum_{t=1}^{M}\sum_{i=1}^{N}\left(X_{it}^{sim} - X_{it}^{obs}\right)^2 + \left(Y_{it}^{sim} - Y_{it}^{obs}\right)^2}{\sum_{t=1}^{M}\sum_{i=1}^{N}\left(X_{it}^{obs}\right)^2 + \left(Y_{it}^{obs}\right)^2}} \tag{14}$$

Among them, t is the time; M is the total time; i is the vehicle; N is the number of non-motorized vehicles; Y_{it}^{sim} is the simulated ordinate of the ith vehicle at time t. Y_{it}^{obs} is the actual ordinate of the ith vehicle at time t; X_{it}^{sim} represents the simulated abscissa of the ith vehicle at time t; and X_{it}^{obs} represents the actual abscissa of the ith vehicle at time t.

The relevant genetic parameters for the calibration of the force correlation model in this paper are as follows: The population size is set to 200, the crossover rate is set to 0.5, the mutation probability is set to 0.1, the maximum evolutionary generation is set to 100,000, and the individual fitness function value is set to 1×10^{-6}. The maximum evolutionary algebra controls the number of iterations. The process is repeated ten times to find a result closer to the global optimum, and the parameter set with the slightest error is chosen [35].

Therefore, Table 2 gives the measurable state parameters and calibration parameters.

Table 2. Measurable state parameters and calibration parameters.

Model	Parameter Type	Parameter	Value	Description
Overtaking force model	Measurable state parameters	V_u	5.27	Average bicycle speed expected (m/s)
			6.25	Average expected speed of electric vehicles (m/s)
		y_d	0.98	The average value of the lateral displacement of the bicycle over the bicycle (m)
			2.06	The average value of the lateral displacement of the electric vehicle over the electric vehicle (m)
			1.28	The average value of the lateral displacement of the bicycle super electric vehicle (m)
			1.18	The average value of the lateral displacement of the electric vehicle overtaking the bicycle (m)

Table 2. *Cont.*

Model	Parameter Type	Parameter	Value	Description
		t_0	1.95	Average overtaking time for bicycles overtaking bicycles (s)
			2.00	Average overtaking time of electric vehicles over electric vehicles (s)
			3.37	Average overtaking time for bicycles over electric vehicles (s)
			2.07	Average overtaking time for electric vehicles overtaking bicycles (s)
	Calibration parameters	n	0.70	Bicycle Overtaking Bicycle Overtaking Coefficient
			1.40	Electric vehicle overtaking electric vehicle overtaking coefficient
			0.70	Bicycle overtaking electric vehicle overtaking coefficient
			0.88	Electric vehicle overtaking bicycle overtaking coefficient
		s_a	2.00	Overtaking interval (s)
Following force model			9.01	Bicycle to bicycle interval (s)
			4.06	The time interval between electric vehicles and electric vehicles(s)
			4.95	Time between bicycles and electric vehicles (s)
			4.45	Time between electric vehicles and bicycles (s)
		a_{max}	1.00	Bicycle maximum acceleration/deceleration speed(m/s^2)
			1.10	Maximum acceleration/deceleration speed of electric vehicle (m/s^2)
		δ_e	2.20	Bicycle and Bicycle Acceleration Index
			1.55	Electric vehicle and electric vehicle acceleration index
			2.03	Bicycle and electric vehicle acceleration index
			0.002	Electric vehicle and bicycle acceleration index
		b_f	1.61	Comfortable deceleration between bicycle and bicycle(m/s^2)
			2.32	Comfortable deceleration of electric vehicles and electric vehicles (m/s^2)
			2.20	Comfortable deceleration of bicycles and electric vehicles (m/s^2)
			1.24	Comfortable deceleration of electric vehicles and bicycles (m/s^2)
		s_0	9.45	Distance from bicycle to bicycle jam0 (m)
			2.65	The distance between electric vehicles and electric vehicles0 (m)
			4.98	The distance between bicycles and electric vehicles0 (m)
			4.76	The distance between electric vehicles and bicycles0 (m)
		s_1	6.23	Distance from bicycle to bicycle jam1 (m)
			3.76	The distance between electric vehicles and electric vehicles1 (m)
			2.01	The distance between bicycles and electric vehicles1 (m)
			4.47	The distance between electric vehicles and bicycles 1 (m)
		T_d	1.34	The time gap between bicycle and bicycle safety time (s)
			1.75	The time gap between electric vehicles and electric vehicles (s)
			1.50	The time gap between the safety time of bicycles and electric vehicles (s)
			2.09	The time gap between electric vehicles and bicycles (s)
Boundary force model		A_{uW}	1.20	Boundary force
		B_{uW}	600	
Driving force model		τ_d	0.20	Buffer time
Repulsive force model		A_{uV}	0.48	Repulsive force
		B_{uV}	600	

3.3. Simulation Results and Discussion

Based on the calibration results, this section will discuss the performance of the proposed model. Simulation results are compared with observations in empirical data with the original SFM [19] simulation performance. Table 2 shows that the calibration parameters of the original SFM are the same as the model's optimal values (for the driving force model, the repulsive force model and the boundary force model).

3.3.1. Speed Analysis

Figure 6 is a video randomly selected for 60 s from the empirical data, and the speed of non-motorized vehicles (electric vehicles and bicycles) at each moment is summarized. The speed distribution map of non-motorized vehicles is obtained. In addition, the simulation experiment takes the speed, position and time of non-motorized vehicles in the empirical data as the starting value. The simulation velocity distribution of non-motorized vehicles is obtained by simulating a free-movement model. The abscissa of the figure represents

the distribution of the speed of non-motorized vehicles, and the ordinate represents the percentage of the total number of vehicles that speed. Average the speeds of electric vehicles and bicycles, respectively, to obtain the expected speeds of electric vehicles and bicycles in this experiment.

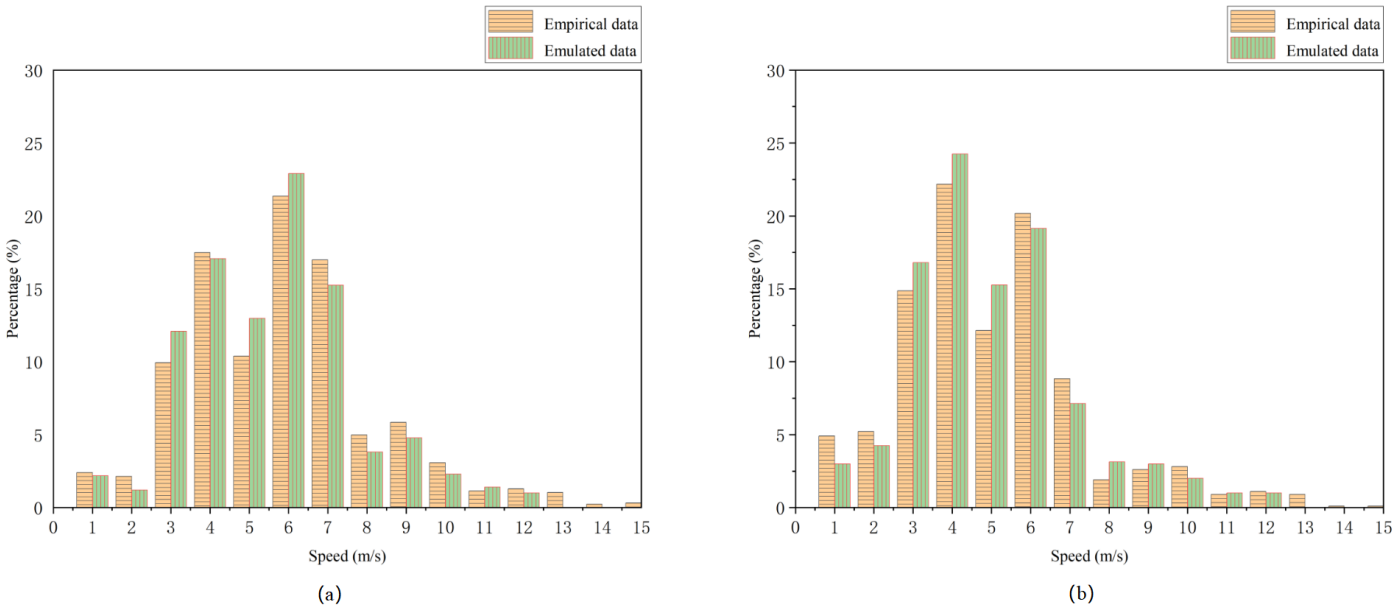

Figure 6. Speed distribution of non-motorized vehicles. (**a**) Electric vehicle speed distribution map. (**b**) Bicycle speed distribution map.

3.3.2. Decision Process Analysis

To reveal and justify the proposed model in determining riders' decision making and interactions, we conduct simulation and empirical data comparisons on the following and overtaking behaviors of riders with significant interaction, discussing changes in their behavioral decisions and their longitudinal and The change of lateral position with time is shown in Figures 7 and 8.

Among them, Figure 7 shows the simulation effect of a randomly selected situation at each moment. Figure 8 shows the decision-making process that the rider follows. Initially, the simulated cyclist is free to move. Timing starts when the following behavior occurs, and the simulated cyclist decides to perform the following behavior. It can be seen from Figure 8 that the following in the simulation is very close to the observed results. The entire simulation motion process is similar to the observed results. It may be because the proposed simulation model can accurately replicate the cyclist's behavioral choices, thus proving the good effect of the following models in the decision-making model.

Among them, Figure 9 shows the effect on the simulation of a random overtaking situation at each point in time. Figure 10 shows the decision-making process of the rider overtaking. Initially, the simulated cyclist is free to move. Timing starts when the overtaking behavior occurs, and the simulated cyclist decides to execute the overtaking behavior. It can be seen from Figure 10 that the overtaking in the simulation is very close to the observation results. The entire simulation motion process is similar to the observed results. It may be because the proposed simulation model can accurately replicate the cyclist's behavioral choices, thus proving the good effects of the overtaking model in the decision-making model.

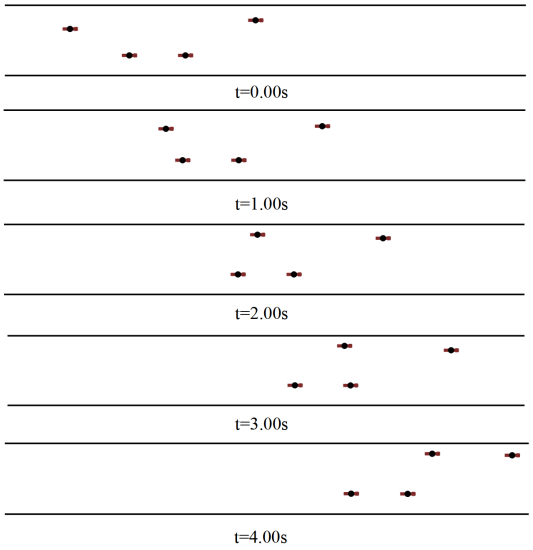

Figure 7. Simulation diagram of a bicycle following a bicycle at each moment.

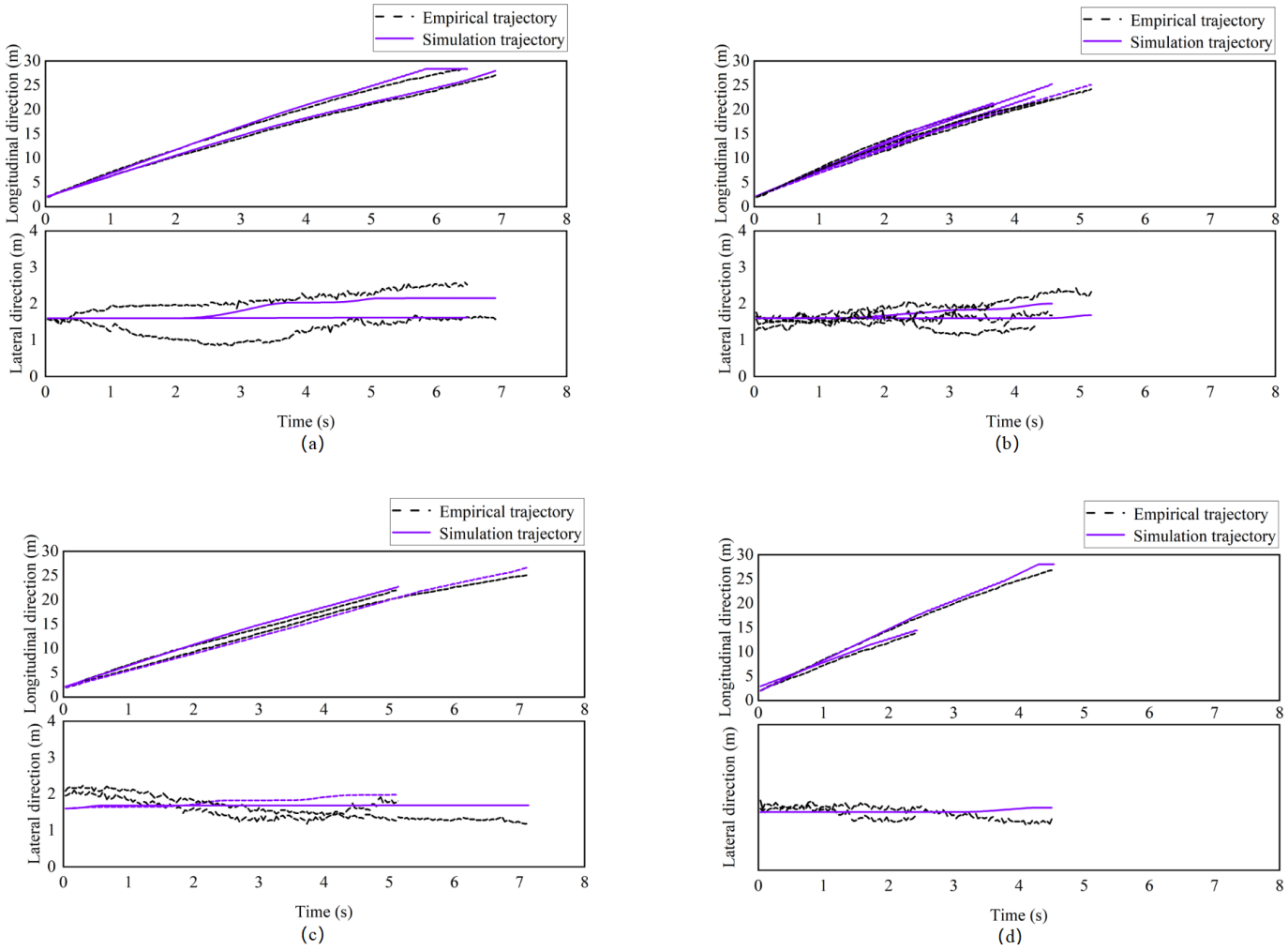

Figure 8. Rider follows the decision-making process. (**a**) Bike following bike. (**b**) Electric vehicles follow electric vehicles. (**c**) Bikes follow electric vehicles. (**d**) Electric vehicle following bicycle.

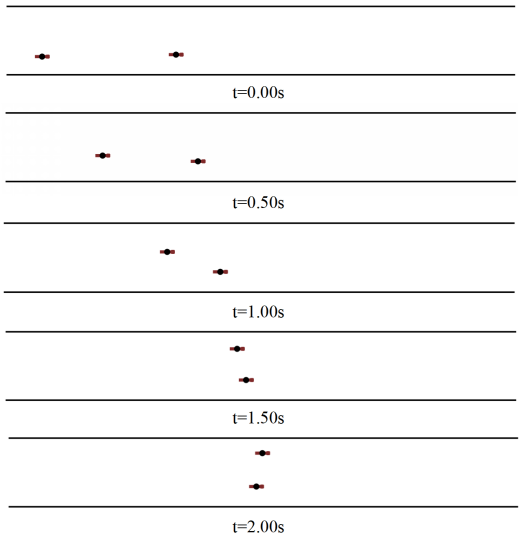

Figure 9. The simulation diagram of each moment of the bicycle overtaking the bicycle.

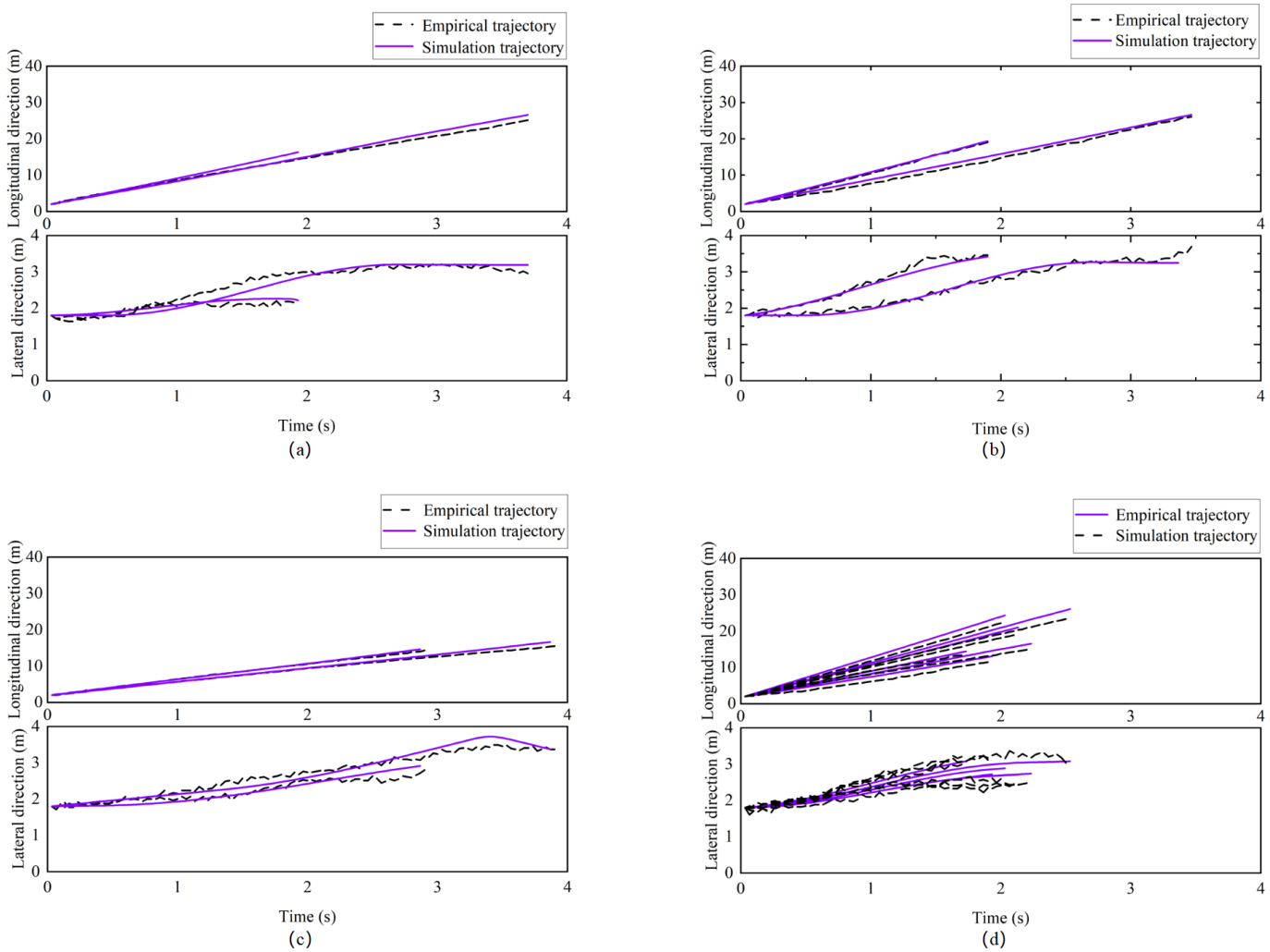

Figure 10. The rider's decision-making process for overtaking. (**a**) Bicycle super bike. (**b**) Electric car super electric car. (**c**) Bicycle ultra electric vehicle. (**d**) Electric vehicle super bike.

3.3.3. Model Comparison

The effect of the bicycle ratio on the average speed of the road is shown in Figure 11. The number of non-motorized vehicles is 5, the abscissa indicates the number of bicycles, and the ordinate indicates the average speed of non-motorized vehicles in the road. We can see that, compared with the original social force model, the average velocity distribution of the improved social force model is closer to the empirical data, with the mean and standard deviation being 5.94 s and 0.74 s, respectively. The mean and standard deviation of the empirical data are 5.96 s and 0.86 s, respectively, and the mean and standard deviation of the original social force model are 5.53 s and 0.44 s, respectively. The results show that the improved social force model outperforms the original social force model in simulating the behavior of non-motorized vehicles due to the dynamic control of the behavioral decision-making process.

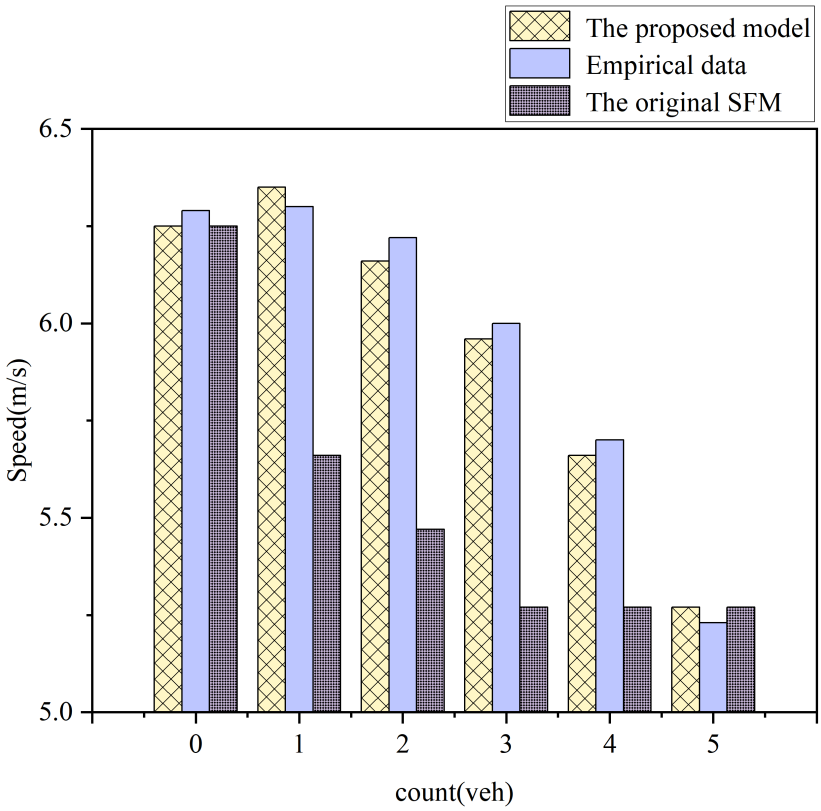

Figure 11. The effect of bicycle ratio on the average speed of the road.

3.4. Model Application

3.4.1. The Influence of Bicycle Ratio on the Speed of Electric Vehicles

Based on the results of calibration and comparison between the simulated trajectory and the actual trajectory, we conducted an applied study on the effect of the bicycle ratio in the road on the average speed of electric vehicles. We set the number of non-motorized vehicles passing through the passage to 5, 15 and 30, respectively, and we discuss the change in the average speed of electric vehicles in the passage by changing the proportion of bicycles.

Analysis of Figure 12 shows that, when there are 5 non-motorized vehicles in the passage, the electric vehicle's speed will increase when the number of bicycles is small due to overtaking. As the number of bicycles increases, bicycles block the passage of electric vehicles, so the speed of electric vehicles decreases significantly.

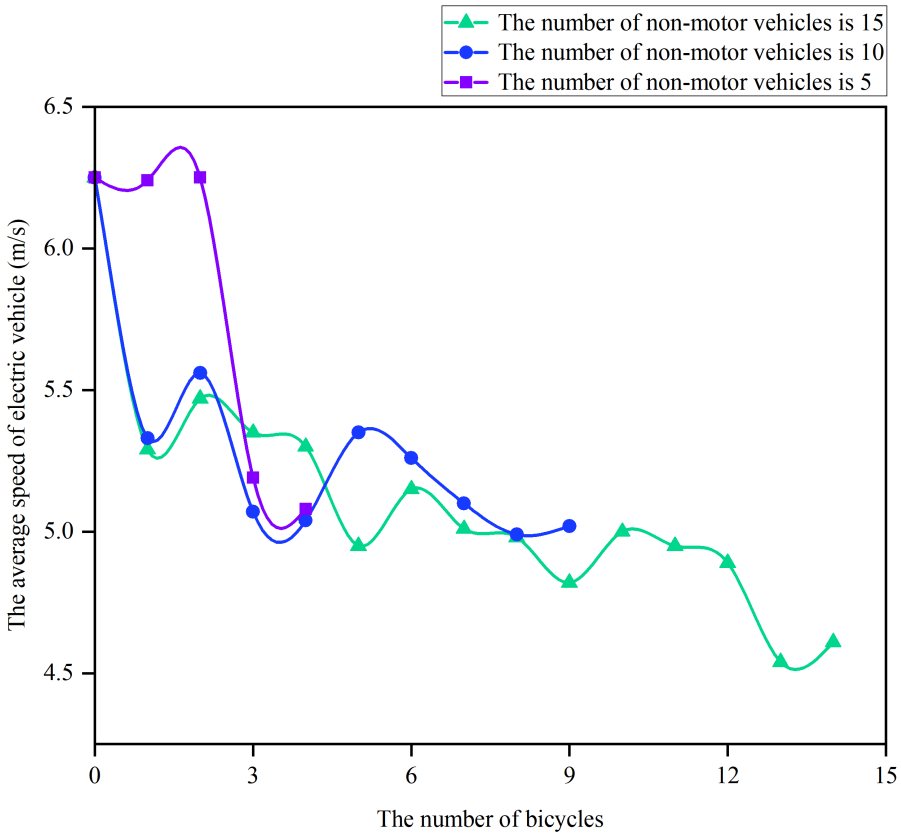

Figure 12. The effect of the number of bicycles on the average speed of electric vehicles.

When the number of non-motorized vehicles in the passage is 10, overtaking is not obvious due to a large number of electric vehicles, which leads to a significant reduction in the speed of electric vehicles when the number of bicycles is small. As the number of bicycles increases, the speed of electric vehicles decreases gradually in fluctuations.

When the number of non-motorized vehicles in the passage is 15, the situation is similar to that of 10. Compared with the number of non-motorized vehicles in the road of 10, the speed of electric vehicles decreased significantly when 15 vehicles were in the road.

When the overall number of non-motorized vehicles is small, a small number of bicycles can promote the traffic efficiency of electric vehicles to a certain extent. When the overall number of non-motorized vehicles is large, the existence of bicycles will reduce the traffic efficiency of electric vehicles. As the proportion of bicycles increases, the traffic efficiency of electric vehicles gradually decreases, and the greater the overall number of non-motorized vehicles, the more pronounced the decline in the traffic efficiency of electric vehicles.

3.4.2. The Impact of the Average Speed of Electric Vehicles on the Overall Traffic Speed

Based on the calibration of the simulated and actual trajectories, we conducted applied research on the relationship between the average speed of electric vehicles and the overall traffic speed. We set the number of non-motorized vehicles passing in the passage to 5, 10 and 15, respectively, and the ratio of the number of electric vehicles to bicycles is 3:2. We discuss the change in overall passing speed in the passage by changing the average speed of electric vehicles.

From the analysis in Figure 13, it can be seen that when the number of non-motorized vehicles in the road is 5, when the speed of electric vehicles is relatively slow, the speed of electric vehicles tends to increase due to the situation involving overtaking. The overall traffic speed of the road will increase accordingly. As the speed of electric vehicles increases,

bicycles hinder the passage of electric vehicles, and the overtaking phenomenon becomes more pronounced. Therefore, the overall passage speed of the road will continue to rise.

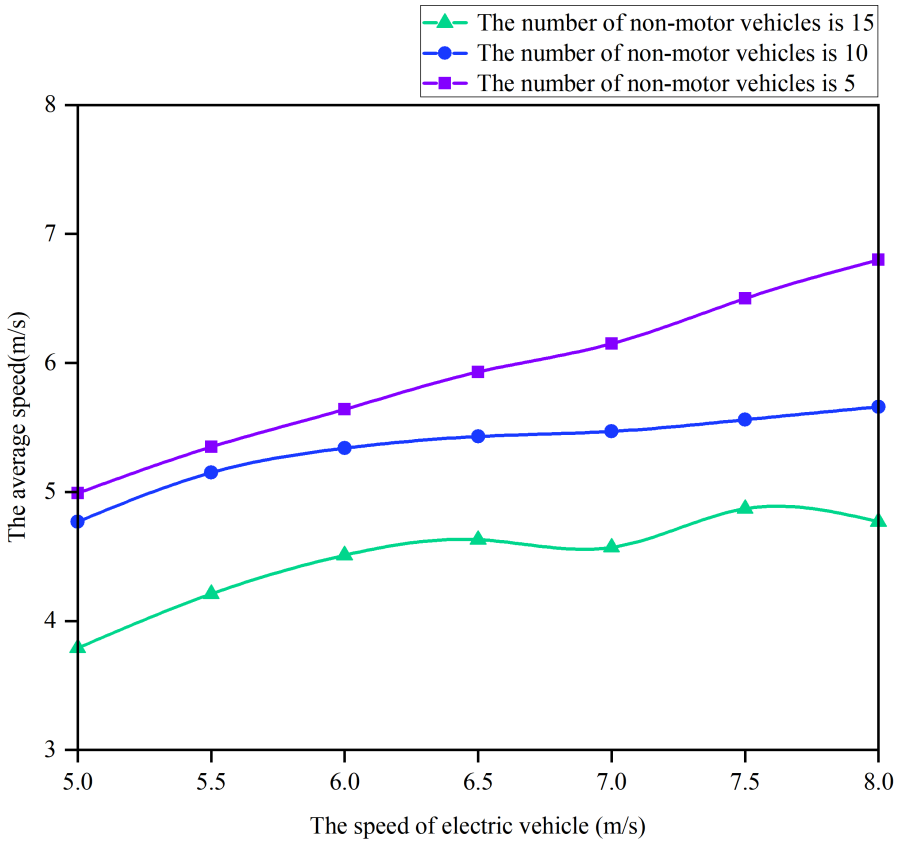

Figure 13. The influence of the average speed of electric vehicles on the overall traffic speed of the road.

When there are 10 non-motorized vehicles in the road, the relationship between the average speed of electric vehicles and the road's overall speed is comparable to that observed when there are 5 non-motorized vehicles. With the increase in the average speed of electric vehicles and the number of non-motorized vehicles in the road, the increase in the overall speed decreases and gradually becomes flat. In addition, the overall passage speed decreased as a whole compared with when the number of non-motorized vehicles was 5.

When the number of non-motorized vehicles in the road is 15, the overall speed of the road will gradually increase due to the large number of non-motorized vehicles. The overtaking phenomenon is not apparent when the speed of electric vehicles is relatively slow. With the increase in the speed of electric vehicles, the overall traffic speed of the road gradually rises, fluctuates less, and finally tends to be flat. With the increase in the number of non-motorized vehicles in the road, the road is more congested, and the overall speed of the road is significantly lower than when the number of non-motorized vehicles is 5.

In the case of a small number of non-motorized vehicles, the increase in the average speed of electric vehicles promotes the overall traffic efficiency of the road. When the number of non-motorized vehicles is large, the number of non-motorized vehicles will significantly affect the overall traffic efficiency. As the number of non-motorized vehicles increases, the average speed of electric vehicles increases, and the overall efficiency of traffic decrease. The greater the number of non-motorized vehicles, the smaller the improvement in the overall traffic efficiency, which eventually tends to be flat.

Based on the application of the above two models, the overall number of non-motorized vehicles, the proportion of bicycles, and the average speed of electric vehicles all have a sig-

nificant influence on the overall traffic efficiency of the road. The number of non-motorized vehicles in the road should, in the case of a specific road width, be kept as close to a specific range as is practical. The average speed of electric vehicles should also be limited to a certain extent.

4. Conclusions

The negative effects of frequent interactions with other cyclists in shared spaces of non-motorized traffic flow greatly affect the safety and efficiency of traffic. Therefore, accurate evaluation tools are needed to meet the urgent needs for facility planning, infrastructure design and traffic management, and microsimulation models are considered effective evaluation tools. However, most existing models greatly simplify the complexity of interactions. Because of this, more changes should be made to meet the requirement of simulating reality as closely as possible.

To address these shortcomings, based on the natural advantages of the original SFM in describing the 2D motion simulation of the cyclist, we embedded a decision model in the original SFM model to represent the interaction between non-motorized vehicles and the dynamics of non-motorized vehicles through the behavioral force decision model. Through simulation, we found that the decision-making process of cyclists' behavior is consistent with reality, which makes up for the lack of decision-making modules in the original SFM. In conclusion, this new microsimulation model can help us figure out how well non-motorized traffic flows, how safe they are and how to design infrastructure.

However, the model proposed in this paper has certain limitations. The model still needs to be expanded with samples to verify its applicability. This model is a microscopic model, which is mainly suitable for simulating the specific behavior of each non-motorized vehicle in a local area. Since the overall behavior is more critical when simulating larger areas (for example, cities with road networks), the model is limited. In addition, this model also needs to consider personal characteristics such as gender, bicycle type and behavior orientation of different cyclists to improve the model's performance. For the determination of model parameters, more empirical data need to be obtained to verify and determine the model's parameters to improve its general applicability. The above shortcomings will be addressed in future work.

Author Contributions: Conceptualization, J.Q. and S.M.; methodology, J.Q.; software, J.Q. and Q.W.; validation, Q.W. and G.F.; formal analysis, J.Q.; investigation, J.Q.; resources, S.M. and L.Z.; data curation, J.Q. and Q.W.; writing—original draft preparation, J.Q.; writing—review and editing, J.Q.; visualization, J.Q. and Q.W.; supervision, S.M. and L.Z.; project administration, S.M.; funding acquisition, S.M. All authors have read and agreed to the published version of the manuscript.

Funding: This work is supported by National Natural Science Foundation of China under Grant 62003127, Natural Science Foundation of Hebei Province under Grant A2020202034, the Youth Foundation of Hebei Education Department under No. QN2020195.

Institutional Review Board Statement: Not applicable.

Informed Consent Statement: Not applicable.

Data Availability Statement: The data is available from the corresponding author of this paper. Data sharing not applicable.

Conflicts of Interest: The authors declare no conflict of interest.

References

1. Gavriilidou, A.; Wierbos, M.J.; Daamen, W.; Yuan, Y.; Knoop, V.L.; Hoogendoorn, S.P. Large-Scale Bicycle Flow Experiment: Setup and Implementation. *Transp. Res. Rec.* **2019**, *5*, 709–719. [CrossRef]
2. Billot-Grasset, A.; Hours, M. How cyclist behavior affects bicycle accident configurations? *Transp. Res. Part F Traffic Psychol. Behav.* **2016**, *41*, 261–276. [CrossRef]
3. Langford, B.C.; Chen, J.; Cherry, C.R. Risky riding: Naturalistic methods comparing safety behavior from conventional bicycle riders and electric bike riders. *Accid. Anal. Prev.* **2015**, *82*, 220–226. [CrossRef] [PubMed]

4. Yuan, Y.; Daamen, W.; Goñi-Ros, B.; Hoogendoorn, S. Investigating cyclist interaction behavior through a controlled laboratory experiment. *J. Transp. Land Use* **2008**, *11*, 833–847. [CrossRef]
5. Tang, T.Q.; Zhang, B.T.; Xie, C.Z. Modeling and simulation of pedestrian flow in university canteen. *Simul. Model. Pract. Theory* **2019**, *95*, 96–111. [CrossRef]
6. Chen, L.; Tang, T.Q.; Huang, H.J.; Wu, J.J.; Song, Z. Modeling pedestrian flow accounting for collision avoidance during evacuation. *Simul. Model. Pract. Theory* **2018**, *82*, 1–11. [CrossRef]
7. Cao, S.C.; Sun, F.Y.; Li, Y. A Cellular Automaton Simulation Model Considering Spatial-temporal Distribution for Mixed Bicycle Flows. *J. Transp. Inf. Saf.* **2022**, *40*, 98–107.
8. Taherifar, N.; Hamedmoghadam, H.; Sree, S.; Saberi, M. A macroscopic approach for calibration and validation of a modified social force model for bidirectional pedestrian streams. *Transp. Transp. Sci.* **2019**, *15*, 1637–1661. [CrossRef]
9. Li, J.; Liu, W.; Zhang, F.; Li, T.; Wang, R. A Ship Fire Escape Speed Correction Method Considering the Influence of Crowd Interaction. *Mathematics* **2022**, *10*, 2749. [CrossRef]
10. Deng, K.; Zhang, Q.; Zhang, H.; Xiao, P.; Chen, J. Optimal Emergency Evacuation Route Planning Model Based on Fire Prediction Data. *Mathematics* **2022**, *10*, 3146. [CrossRef]
11. Huang, L.; Gong, J.; Li, W.; Xu, T.; Shen, S.; Liang, J.; Feng, Q.; Zhang, D.; Sun, J. Social force model-based group behavior simulation in virtual geographic environments. *ISPRS Int. J. Geo-Inf.* **2018**, *7*, 79. [CrossRef]
12. Han, Y.; Liu, H. Modified social force model based on information transmission toward crowd evacuation simulation. *Physica A* **2017**, *469*, 499–509. [CrossRef]
13. Guo, Y.; Ma, S.; Wei, F.; Lu, L.; Sun, F.; Wang, J. Analysis of Behavior Characteristics for Pedestrian Twice-Crossing at Signalized Intersections Based on an Improved Social Force Model. *Sustainability* **2022**, *14*, 2003. [CrossRef]
14. Qin, X.; Liu, H.; Zhang, H.; Liu, B. A collective motion model based on two-layer relationship mechanism for bi-direction pedestrian flow simulation. *Simul. Model. Pract. Theory* **2018**, *84*, 268–285. [CrossRef]
15. Zhou, X.; Ji, Y.; Yuan, Y.; Zhang, F.; An, Q. Spatiotemporal characteristics analysis of commuting by shared electric bike: A case study of Ningbo, China. *J. Clean. Prod.* **2022**, *362*, 132337. [CrossRef]
16. Li, M.; Chen, T.; Du, H.; Ma, N.; Xi, X. The speed and configuration of cyclist social groups: A field study. *Phys. A Stat. Mech. Appl.* **2022**, *592*, 126849. [CrossRef]
17. Liu, Q.; Lu, L.; Zhang, Y.; Hu, M. Modeling the dynamics of pedestrian evacuation in a complex environment. *Phys. A Stat. Mech. Appl.*. **2022**, *585*, 126426. [CrossRef]
18. Liu, M.; Chen, T.; Matunaga, C.; Oeda, Y.; Sumi, T. Simulation of dispersion effects by considering interactions of pedestrians and bicyclists using an agent space model. *Comput. Environ. Urban Syst.* **2022**, *91*, 101725. [CrossRef]
19. Anvari, B.; Bell, M.; Sivakumar, A.; Ochieng, W.Y. Modelling shared space users via rule-based social force model. *Transp. Res. Part C Emerg. Technol.* **2015**, *51*, 83–103. [CrossRef]
20. Luo, L.; Luo, Y.; Feng, Y.; Li, T.; Fu, Z. Experimental investigation on pedestrian–bicycle mixed merging flow in T-junction. *Phys. A Stat. Mech. Appl.* **2022**, *600*, 127492. [CrossRef]
21. Schöttl, J.; Seitz, M.J.; Köster, G. Investigating the randomness of passengers' seating behavior in suburban trains. *Entropy* **2019**, *21*, 600. [CrossRef] [PubMed]
22. Han, Y.; Chao, Q.; Jin, X. A simplified force model for mixed traffic simulation. *Comput. Animat. Virtual Worlds* **2021**, *32*, e1974. [CrossRef]
23. Lü, Y.X.; Wu, Z.X.; Guan, J.Y. Pedestrian dynamics with mechanisms of anticipation and attraction. *Phys. Rev. Res.* **2020**, *2*, 043250. [CrossRef]
24. Qu, Z.; Cao, N.; Chen, Y.; Zhao, L.; Bai, Q.; Luo, R. Modeling electric bike–car mixed flow via social force model. *Adv. Mech. Eng.* **2017**, *9*, 1687814017719641. [CrossRef]
25. Ma, Z.; Sun, J.; Wang, Y. A two-dimensional simulation model for modelling turning vehicles at mixed flow intersections. *Transp. Res. Part C* **2017**, *75*, 103–119. [CrossRef]
26. Liang, X.; Xie, M.; Jia, X. New Microscopic Dynamic Model for Bicyclists' Riding Strategies. *J. Transp. Eng. Part A Syst.* **2018**, *144*, 04018034. [CrossRef]
27. Helbing, D.; Molnar, P. Social force model for pedestrian dynamics. *Phys. Rev. E* **1995**, *51*, 4282–4286. [CrossRef] [PubMed]
28. Li, Y.X.; Ni, Y.; Sun, J. A modified social force model for high-density through bicycle flow at mixed-traffic intersections. *Simul. Model. Pract. Theory* **2021**, *108*, 102265. [CrossRef]
29. Li, Y.X.; Ni, Y.; Sun, J.; Ma, Z. Modeling the illegal lane-changing behavior of bicycles on road segments: Considering lane-changing categories and bicycle heterogeneity. *Phys. Stat. Mech. Its Appl.* **2020**, *541*, 123302. [CrossRef]
30. Hoogendoorn, S.; Daamen, W. Bicycle Headway Modeling and Its Applications. *Transp. Res. Rec. J. Transp. Res. Board* **2016**, *2587*, 34–40. [CrossRef]
31. Jin, S.; Qu, X.; Zhou, D.; Xu, C.; Ma, D.; Wang, D. Estimating cycleway capacity and bicycle equivalent unit for electric bicycles. *Transp. Res. Part A Policy Pract.* **2015**, *77*, 225–248. [CrossRef]
32. Gavriilidou, A.; Daamen, W.; Yuan, Y.; Hoogendoorn, S.P. Modelling cyclist queue formation using a two-layer framework for operational cycling behaviour. *Transp. Res. Part Emerg. Technol.* **2019**, *105*, 468–484. [CrossRef]
33. Treiber, M.; Hennecke, A.; Helbing, D. Congested traffic states in empirical observations and microscopic simulations. *Phys. Rev. E* **2000**, *62*, 1805. [CrossRef]

34. Treiber, M.; Kesting, A. The intelligent driver model with stochasticity-new insights into traffic flow oscillations. *Transp. Res. Procedia* **2017**, *23*, 174–187. [CrossRef]
35. Zhu, M.; Wang, X.; Tarko, A.; Fang, S. Modeling car-following behavior on urban expressways in Shanghai: A naturalistic driving study. *Transp. Nat. Res. C Emerg. Technol.* **2018**, *93*, 425–445. [CrossRef]